

Augmented Collisional Ionization in the VUV regime; a theoretical study

Nicolas Bigaouette* and Lora Ramunno†

Department of Physics, University of Ottawa, 150 Louis Pasteur, Ottawa ON, K1N 6N5, Canada

Edward Ackad‡

*Department of Physics, Southern Illinois University Edwardsville,
State Route 157 Edwardsville, IL 62026, United States*

(Dated: August 25, 2013)

We revisit a major 2002 experiment at FLASH-DESY FEL facilities on Xenon clusters interacting with VUV (98 nm, 12.65 eV) 100 fs laser pulses. Previously thought to have an intensity of 2×10^{13} W/cm² it was later re-calibrated in 2010 to 8×10^{12} W/cm², less than half the initial value. In light of this new intensity, we revisit this experiment in the VUV regime by applying our Augmented Collisional Ionization (ACI) model. Included also is single photon ionization, impact ionization and (in some simulations) recombination. At this wavelength and intensity, tunnel and multi-photon ionization are negligible and are thus not included. We found that ACI increases both the maximum charge state seen and the most abundant one, both by two states higher. ACI was required to match the experimental data. A deeper potential depth as used in other studies revealed a large influence on charge state spectra.

August 25, 2013

I. INTRODUCTION

The advance of Free Electrons Lasers (FEL) around the world gave access to unprecedented intensity at wide range of wavelengths, including from the VUV to X-ray. Recent experiments have studied the interaction of such laser pulses with clusters of atoms. These clusters are nanoscopic objects at solid density. Additionally, their finite size makes them easier to study, both theoretically and experimentally.

Many studies of the interaction of laser-matter have been done at wavelengths ranging from the IR to X-ray regimes. Experiments in 2002 by Wabnitz *et al.*[1] at FLASH-DESY FEL facilities on clusters of Xenon and VUV radiation saw surprisingly high charge states (Xe⁸⁺) using 98 nm (12.7 eV). The heating and ionization mechanisms known at that time could not explain the high charge states; more work was required. Three major models emerged to explain these high ionization levels.

First, the lowering of the potential barrier was suggested for photo-ionization [3–6] where a neighbouring ion lowers the barrier, making the absorption of a single photon by the electron energetically possible.

Second, Santra and Green suggested using atomic potential instead of the Coulomb potential. They used a simple screening potential [7] and later a more realistic one [8] based on a Hartree-Fock-Slater code written by F. Herman and S. Skillman [9] and saw 30 times more VUV photons absorbed by a cluster environment compared with using a Coulomb potential. Charge states up

to Xe⁶⁺ for Xe₁₅₀₀ clusters were obtained with simulations using the atomic potentials.

Jungreuthmayer *et al.*[2] identified an additional mechanism dubbed “Multi-Body Recombination” (MBR) heating. Through laser-cluster simulations based on classical dynamics, they showed that the created plasma is cold and dense enough to fall within the strongly coupled plasma regime. As such, the plasma is highly collisional and via multiple collisions electrons can recombine to a highly excited state with high probability. This newly recombined electron can then reabsorb a new photon from the laser, effectively increasing the system’s energy absorption from the laser.

In 2010, the intensity of the DESY-FEL pulses[1] was re-calibrated to be 40% of the originally quoted value [10]. The question now arises: given that the previous models showed good agreement with experimental result at the originally quoted intensity, is there something potentially missing from the previous models in light of this intensity adjustment? In this paper, we investigate two possible effects that might contribute.

First, our group recently investigated the involvement of atomic excited states in collisional ionization in laser-cluster interaction experiments in the XUV[11–13]. We presented a model wherein collisional ionization is allowed to occur in two steps. First, a colliding electron may promote a bound electron to an excited state. Then another colliding electron may promote this excited one into the conduction band. This allows lower-energy electrons to ionize an atom/ion, where such ionization would not be possible via the usual single-step collisional ionization models. We called this process “Augmented Collisional Ionization” (ACI), and we now seek to investigate its role in the VUV laser-cluster regime. We do this via a classical model similar to that employed by Jungreuthmayer *et al.*

Second, we investigate the effect of the electron-ion

* nbigaouette@gmail.com

† lramunno@uottawa.ca

‡ eackad@siue.edu

potential in classical simulations, given the large effect of potential shape on VUV-cluster interaction found by Santra and Green. Though in this work we only use the Coulomb potential, we investigate how the potential depth of the softened version affects simulation outcomes. This provides some hints as to how a different potential shape may interact with classical simulations.

In the first part of this paper, we will describe our classical approach to the clusters' dynamics followed by the different ionization processes which are treated quantum mechanically. Results are then presented by first showing the influence ACI has on the maximum charge states seen in simulations. Then, the cluster size influence is studied and compared to experiments by averaging over the spatial distribution of the laser pulse. Last, we investigate the influence of the potential depth used in our simulations on the maximum charge state seen.

II. MODEL

Clusters are nanoscopic systems and as such are hard to model using statistical approaches which often assume infinite systems. Our model thus tracks every particle present using a classical molecular dynamics (MD) code. Such MD codes are excellent tools for the simulation of a low number of particles since no approximation is used (apart from the classical instantaneous electrostatic interactions). Unfortunately, the N-body problem has no analytic solutions and is chaotic, requiring large amount of data for valid statistics. Furthermore, the MD interaction calculation has an $O(N^2)$ scaling which renders simulations of tens of thousands of particles using long range interactions virtually impossible. Approximations to the N-body problem are possible; hierarchical tree code [14] and fast-multipole methods [15] can reduce the burden to an $O(N \log(N))$ problem.

These algorithms have overheads which makes them slower for a lower number of particles. They can also introduce some errors in the force and potential calculations. While these errors are not significant for the dynamics aspect of the simulation, they can influence the calculated rates of quantum transitions. We instead decided to port the classical dynamics aspect of the simulation to the OpenCL framework. This allows us to accelerate calculation on general-purpose graphical processing units (GP-GPU), bringing a speed up of between 40 and 80 times.

The Coulomb interaction between particles is softened at small distances to avoid numerical errors due to the singularity. Particles are treated as Gaussian charge densities where the potential is given by (in atomic units):

$$\phi(r) = \frac{Z}{r} \operatorname{erf}\left\{\frac{r}{\sigma\sqrt{2}}\right\} \quad (1)$$

with erf the error function, Z the charge state of the

particle and σ the width of the charge density given by:

$$\sigma = \frac{Z}{D} \sqrt{\frac{2}{\pi}} \quad (2)$$

The maximum depth of the potential of a $Z = 1$ ion is given by the parameter D . At large distances ($r \gg \sigma$), this smoothed potential converges to the Coulomb potential.

Initially, the simulated cluster is a collection of neutral atoms. As time passes, the laser is modelled as both an oscillating electric field with a carrier envelope and a flux of photons. Electrons and ions are created in the code by ionization events modelled via quantum rates. These are now described in the following section.

A. Single photon ionization

The first step in the interaction is single photon ionization of the neutral atoms. As such ionization events occur, the laser amplitude is depleted. Experimental cross sections for Xenon in the VUV regime were taken from experimental data [16]. These cross-sections are converted to rates and a Monte-Carlo test evaluates the ionization probability.

At the studied intensities (10^{12} to 10^{13} W/cm²) and wavelength (98 nm, 12.65 eV), tunnel ionization is negligible, as is multi-photon absorption. In addition, ions cannot be further ionized via single photon ionization.

B. Threshold V_p

Many processes are modelled using quantum rates known for isolated atoms. For example, the semi-empirical Lotz cross-sections for impact ionization assumes the impacting electron comes from infinity where its potential energy is null. However the cluster environment must be taken into account. We model these interactions as those of an isolated system residing in a constant potential created by the cluster environment. This potential V_p is the contribution of all particles outside the nearest neighbour distance in the pre-ionized cluster.

C. Impact ionization

Impact ionization is implemented using the semi-empirical Lotz cross-sections[17] with parameters taken from references [18] for the neutral and [19] for ionized Xenon. The impact parameter b of the impacting electron is calculated through $b = |\mathbf{v} \times \mathbf{r}| / |\mathbf{v}|$ where \mathbf{v} is the impacting electron's velocity vector and \mathbf{r} the vector from the impacting electron to the target. If the impact parameter lies inside the calculated cross section, ionization takes place. We take the impacting electron's total energy with respect to the threshold V_b as its effective kinetic energy.

D. Augmented Collisional Ionization (ACI)

In recent work, we introduced a model [12] which we dubbed “Augmented Collisional Ionization” (ACI) that we applied to Argon experiments at 32.8 nm [20] and Xenon clusters in soft X-rays (13.7 nm, 90.5 eV) [13, 21]. We now port that model over to the VUV regime.

In the ACI model, electrons are created in a two step process. After an electron collides with an atom or ion, we allow for the final state to be an excited atom or ion plus a reduced-energy impact electron. Once excited, an atom or ion can be impact-ionized more easily by a second, lower energy, impacting electron. ACI thus allows electrons in the lower energy tail of the kinetic energy spectrum to contribute to the cluster ionization. Additionally, more ionization paths are present in the model.

ACI is modelled similarly to impact ionization. Cross sections for the different transitions are taken from a Hartree-Fock implementation of the Cowan code [22]. For this work on Xenon clusters, eight excited states ($l < 4$) per charge state are used, for ionization levels up to Xe^{17+} .

E. Ground state recombination

We include in our model recombination to the ground state as described in detail in our previous work [13]. If an electron’s total energy with respect to the V_p threshold becomes lower than the ground state energy, this electron is recombined with the parent ion and disappears from the simulation. The ion’s charge state is updated to reflect the process.

This allows having a potential that is as close as Coulombic as possible (except at really close range where the potential converges to $\phi = ZD$) without having electrons with classical energy below the ground state. Interestingly, it also accelerates the $O(N^2)$ force calculation by reducing the number of particles in the system.

F. Many Body Recombination

MBR is automatically included in a classical MD simulation and is thus included in our results.

An important distinction between MBR and ACI is the direction in which the electronic transition takes place. In the case of ACI, the transition is going “up the energy ladder”: a bound electron first in the ground state will receive energy from an impacting electron. Afterwards, the excited atom is ionized more easily by other impacting electrons due to, firstly, the cross-section of the excited state to continuum state being larger than the cross-section from the ground state to continuum. Secondly, the energy required for the excited state to continuum transition is less than that of the ground state to continuum transition and as such more free electrons have a chance to ionize the excited atom. On the other

hand, MBR is a transition from the continuum to a highly excited state. While the later is treated purely classically, the former is implemented using cross-sections taken from a Hartree-Fock calculation. The lower excited states used in ACI are distant from each other and must be treated discretely while the higher states in MBR are so dense that their classical treatment does not result in much error.

III. RESULTS

When irradiated with a 98 nm (12.95 eV) laser pulse, the cluster becomes fully ionized rapidly. This is due to the fact that single photon ionization cross-section is largest (68 Mb) at this longer wavelength for neutral Xenon. Since the photon energy is not sufficient to ionize a Xe^{1+} to a Xe^{2+} , only the first charge state is accessible through single photon ionization. Larger charge states are caused by other mechanisms as is evidenced by experiments with gas targets.

Similarly to reference [2], the Coulomb potential is cut-off at close range to prevent the large field close to the discontinuity to cause numerical heating. Equation (1) is used for the cut-off with $D = 12$ eV. Such a shallow value is used to compare with previous publications where recombination is not present. Even though in a classical simulation an electron orbiting in a Coulomb potential can have a range of energy from zero to minus infinity, fixing the maximum depth of the potential to 12 eV prevents the orbiting electron from having a classical energy less than the recombination energy. Allowing an electron to have an energy below this recombination threshold value would also allow the electron to transfer its energy to other particles, artificially heating the system. This problem is prevented by simply choosing a potential depth D close to the ionization potential of the neutral Xenon.

The small nature of these clusters, the random process of the Monte-Carlo ionization procedures and the chaotic nature of the many-body problem requires acquiring a large sample for valid statistics; for small clusters, 5,000 simulations were run for both ACI disabled and enabled. For larger clusters 100 simulations were performed for both ACI disabled and enabled.

The cluster dynamics after the laser pulse is mainly an expansion; no significant ionization has been observed during that time. As such, simulations were run up to 400 fs which is approximately 150 fs after the end of the laser pulse. We have not seen any major changes when continuing the simulations to longer times.

Cross-sections used in this work were taken from experimental data from reference [16] for single photon ionization. For impact ionization, experimental cross-sections from references [18] and [19] rather than Lotz [17] were used.

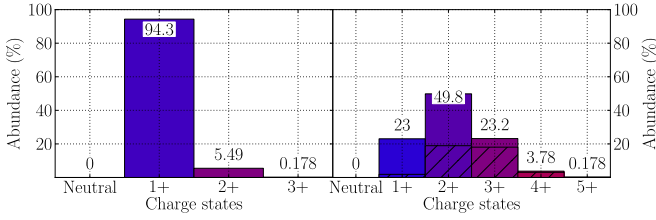


FIG. 1: Charge states spectra of Xe_{90} clusters at $8 \times 10^{12} \text{ W/cm}^2$ with ACI disabled (left) and enabled (right)

A. ACI influence on highest charge state

We first compare the highest charge states seen in both our simulations and the 2002 experiment at DESY. We ran simulations on Xe_{90} clusters to compare with figure 1 of Wabnitz *et al.*. Additionally, the intensity of the 2002 experiment was re-calibrated in 2010[10] from 2×10^{13} to $8 \times 10^{12} \text{ W/cm}^2$, around 40 % of the initial value. We thus ran our simulations at the lower, revised intensity.

Figure 1 shows the resulting charge state spectrum. The left subplot shows data when ACI is not enabled, while the right subplot shows the spectrum when ACI is enabled, with the ratio of excited states in hatched regions.

As we can see, ACI increases by two the maximum charge state from Xe^{3+} to Xe^{5+} . The 2002 experiment showed a clear signal for at least Xe^{4+} for Xe_{80} clusters. We could barely see a Xe^{3+} in our simulations without ACI ($\sim 0.2\%$) while a Xe^{4+} is clearly seen when ACI is enabled, similarly to the experimental data.

At the (revised) intensity of $8 \times 10^{12} \text{ W/cm}^2$, the next larger clusters are $\text{Xe}_{30,000}$ (revised in 2010 to $\text{Xe}_{90,000}$) which are not accessible in our simulations due to computational limitations. Data for $\text{Xe}_{1,500}$ was presented in [1] but at the larger intensity of $7.3 \times 10^{13} \text{ W/cm}^2$. If the same re-calibration is applied to this intensity, we can compare with our simulation results of $\text{Xe}_{1,000}$ at $1.5 \times 10^{13} \text{ W/cm}^2$ shown on figure 2. When ACI is disabled, the maximum charge state seen is Xe^{5+} but at an insignificant ratio ($\sim 0.01\%$) that would be lost in the noise of experimental data. On the contrary, some Xe^{7+} is found when ACI is enabled (with Xe^{6+} being more realistic), an increase of 2. Experimental data shows a maximum of Xe^{8+} .

This is a clear indication that ACI plays a vital role in the dynamics and cannot be ignored when experiments are discussed.

We also measured the number of electrons which are in a Many-Body Recombination (MBR) state. We found that around 18 % of the total number of electrons are in an MBR state, close to the value from reference [2] (around 25 %), an indication that MBR is still important in the description of the dynamics.

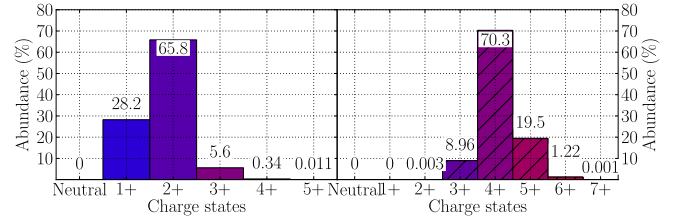


FIG. 2: Charge states spectra of Xe_{1000} clusters at $1.5 \times 10^{13} \text{ W/cm}^2$ with ACI disabled (left) and enabled (right)

Distance to focus	Normalized height	Intensity ($\times 10^{12} \text{ W/cm}^2$)
0	1	8.000
$\sqrt{-2\sigma^2 \ln\left(\frac{1+e^{-1/2}}{2}\right)}$	$\frac{1+e^{-1/2}}{2}$	6.424
σ	$e^{-1/2}$	4.852
$\sigma\sqrt{2 \ln(2)}$	$1/2$	4.000
$\sqrt{2}\sigma$	e^{-1}	2.943
2σ	e^{-2}	1.083

TABLE I: Intensity of laser pulse at different distances of the focus assuming a gaussian spatial profile with a standard deviation σ .

B. Laser spacial profile

The previous results can only predict the highest charge state seen. For more precise spectra the spacial profile of the laser must be considered.

We assume here that the density of clusters coming out of the nozzle is constant in space over the whole laser focus. As such, the clusters distributed across the focus' spatial profile will sample a different laser intensity depending on their distance from the focus' centre. This is taken into account by running many simulations at different intensities. Each intensity is then weighted accordingly to represent the different location in the laser's focus two dimensional cross section profile.

The peak intensity of the experiment being $8 \times 10^{12} \text{ W/cm}^2$, we chose the values for the simulations shown on table I. Considering a focus diameter (FWHM) of $\tau = 20 \mu\text{m}$ we have $\sigma = \tau \left(2\sqrt{2 \ln(2)}\right)^{-1} = 11.77 \mu\text{m}$.

We study the influence of the cluster size on the charge states spectra similarly as figure 1 from Wabnitz *et al.* (or figure 2 from reference Bostedt *et al.*) but due to computational resources limits, the largest clusters simulated were $\text{Xe}_{5,083}$.

Figure 3a shows the charge state distribution for Xe_{90} clusters and figures 3b, 3c and 3d show the distribution of icosahedral clusters with their 7th, 8th and 11th closed shells ($\text{Xe}_{1,415}$, $\text{Xe}_{2,057}$ and $\text{Xe}_{5,083}$, respectively). All icosahedral configurations were relaxed using a Lennard-Jones potential for neutral xenon.

It is important to remember here that there is no recombination during the simulation. As such, the number of electrons can only increase. While interesting to study the dynamics during the laser pulse, special care needs to be taken when comparing with experiments. Indeed, during the expansion of the cluster (between the end of the laser pulse and the detection on the time-of-flight (TOF) spectrometer) the created plasma will cool down and many electrons will recombine. One cannot thus simply compare the charge state spectrum generated by a simulation and one measured in a TOF. To reduce this difference between the two spectra, we recombine, at the end of every simulations, electrons that are close to an ion and have a negative energy. This energy is calculated as the electron's kinetic energy plus the potential energy between this electron and the nearby ion. Once this recombination is done, the spectra are calculated and plotted on figures 3

Each figure shows the results of our simulations using the same parameters as the DESY-FEL experiment [1, 10] and all intensities shown on table I. For the smallest cluster size (Xe_{90} on figure 3a), ACI increases the highest charge states by one, from Xe^{3+} to Xe^{4+} . For the next larger clusters ($\text{Xe}_{1,415}$), ACI increases the highest charge state observed by two, from Xe^{3+} to Xe^{5+} . Finally, the two largest cluster sizes ($\text{Xe}_{2,057}$ and $\text{Xe}_{5,083}$) see their largest charge state increase from Xe^{4+} to Xe^{5+} when ACI is enabled.

Additionally, the most abundant charge state is shifted from Xe^{1+} to Xe^{2+} when ACI is enabled for large clusters, while staying at Xe^{1+} for the smallest (Xe_{90}) clusters.

Figures 3a, 3b, 3c and 3d are in good agreement with the DESY experiment [1, 10]: the dominant charge states seen was Xe^{2+} for the largest clusters ($\text{Xe}_{90,000}$) while for the smallest (Xe_{70}) the Xe^{1+} ion was dominant.

We can see that figures 3b, 3c and 3d are quite similar except from the fact that the distribution is shifting to larger values as the cluster size increases. Without ACI, the populations of Xe^{3+} goes from 0.28 to 0.35 to 0.59 percent as the cluster size increase from $\text{Xe}_{1,415}$ to $\text{Xe}_{2,057}$ to $\text{Xe}_{5,083}$. The Xe^{3+} population doubles between the $\text{Xe}_{1,415}$ and $\text{Xe}_{5,083}$ clusters.

Even though $\text{Xe}_{5,083}$ clusters are less than four times larger than $\text{Xe}_{1,415}$, they have 4 more closed shells. The doubling of the Xe^{3+} is likely caused by the number of ions on the cluster surface increasing more slowly than the number of ions in the cluster volume. For example, the $\text{Xe}_{1,415}$ clusters have 35 % of atoms inside their volume, while this proportion drops to 24 % for $\text{Xe}_{5,083}$. Since we have seen that the higher charge states reside on the cluster boundaries, as reported in [11], we expect to see a slower increase of the yield of the highest charge states compared to the cluster size increase.

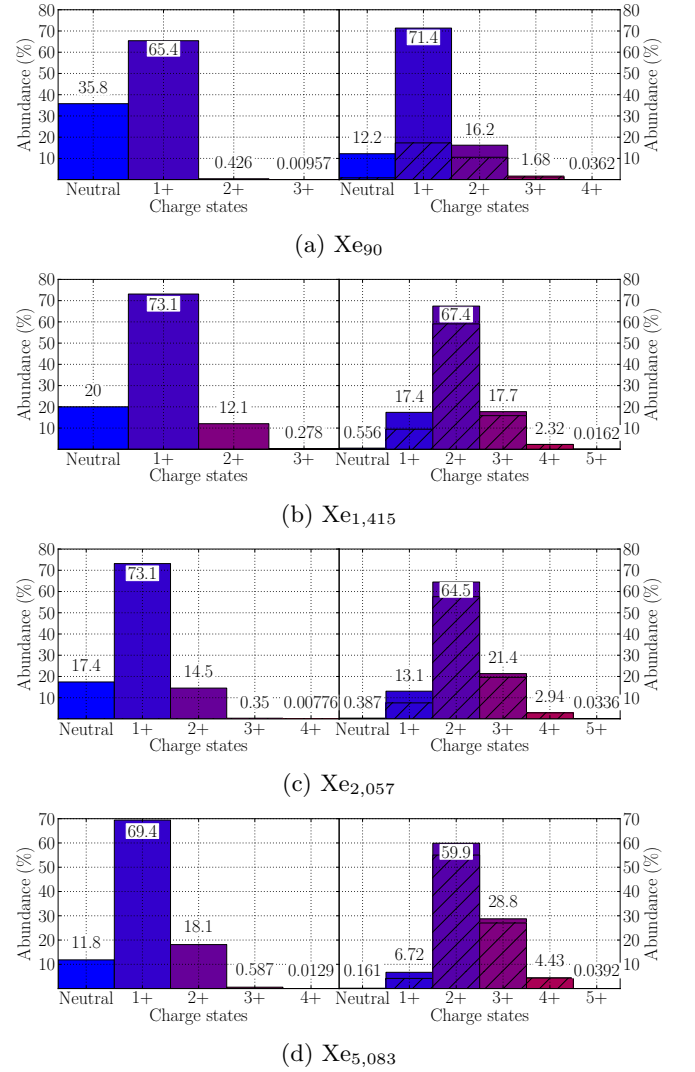


FIG. 3: Charge states spectra of different cluster sizes using intensities of table I. ACI disabled (left) and enabled (right)

C. Effect of deeper potentials

The potential depth of 12 eV used for the cutoff is arbitrary. In reality, electrons will feel a complete potential. However, due to the classical nature of our model, using an infinite potential (for example Coulombic) would allow electrons to fall too deep, causing un-physical heating of the other electrons due to energy conservation.

As suggested in previous studies[7, 8] the shape and depth of the ion potential does have an influence on the dynamics. Using a deeper potentials will allow a larger scattering angle required for heating of the cluster through IBH. To explore this avenue, we now need to used recombination as described in our previous work[13]. This allows using a deeper potential while preventing un-physical events.

As the potential gets deeper, the field close to the ion

increases and a smaller time step must be used. For such deep potentials, the limit on the floating point precision of the computer becomes apparent and decreasing the time step used does not decrease the error anymore. Additionally, simulations using a time step smaller than 0.05 attosecond become intractable as the simulations time increase to many months.

We have thus settled on a time step of 0.15 as which minimizes the calculation error while still providing reasonable simulation duration. We compared the following results with a time step of 0.1 as and found only negligible differences in the charge states distribution.

Additionally, since recombination will change the charge state distribution even after the laser has passed by redistributing energy throughout the cluster, simulations must be run for a longer time. In this case, simulations went up to 1 ps where the cluster is fully exploded.

We find that the depth of the potential does have an influence on the cluster dynamics. We note that no spacial averaging (as in the previous subsection) was performed here. As the potential gets deeper, a smaller time step must be used which slows down simulations significantly. We thus only compare the highest charge states in the spectra.

Figures 4a and 4b show the results for Xe_{80} clusters under a $8 \times 10^{12} \text{ W/cm}^2$ laser pulse for a potential depth D of 27.2 eV (1 Eh) and 81.63 eV (3 Eh) – see equation (2). Refer to figure 1 for a depth of 12 eV (0.441 Eh). We clearly see an increase in both the maximum and dominant charge state seen as the potential depth gets deeper. While the shallow potential depth of 12 eV gives interesting results, we see that a deeper potential is required to obtain higher charge states. We also see that at $D = 3 \text{ Eh}$, the distribution is similar to the one at $D = 1 \text{ Eh}$, an indication of the saturation of the energy absorption. It is thus not necessary to go deeper than 1 Eh to extract the full dynamic of the cluster.

These results can be explained by the increase in IBH due to the electrons being able to sample a deeper ion potential. Though the potential used here is Coulombic, it is similar in idea to what Santra and Greene suggested[7, 8] where the deeper parts of the potential do contribute significantly.

Note that due to the smaller time step used in this section not as many runs could be performed as was done in the previous section; 60 runs were used to generate every charge state spectrum shown on figures 4

IV. CONCLUSION

In summary, many refinements were made on previous models. For example, a smoother shape of the close range potential was used, removing the need for extremely small time steps to keep numerical heating under control. Additionally, the classical dynamics part of the code was re-written to run on GP-GPU using OpenCL for a 40 to 80 times speed increase. This allowed us to increase the

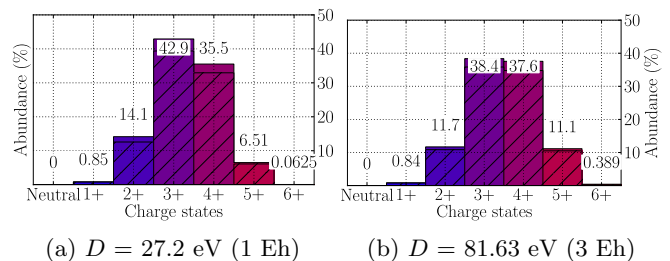


FIG. 4: Charge state spectra after 1 ps of Xe_{80} using an intensity of $8 \times 10^{12} \text{ W/cm}^2$ and different potential depths D (see equation (2)). ACI is enabled for both figures.

number of simulations we ran and thus their statistical significance or to push the simulations size. We could also explore the laser intensity profile by running different simulations at different intensities, proportional to the focal cross section area.

Furthermore, better approximations were made for both single photon and collisional ionization by directly using experimental cross-sections. More importantly, we applied our ACI model that was developed at a different wavelength regime.

We first studied the influence of ACI on the maximum charge states seen for Xe_{80} clusters at $8 \times 10^{12} \text{ W/cm}^2$ and Xe_{1000} clusters at $1.5 \times 10^{13} \text{ W/cm}^2$. We have shown that the maximum charge state seen was increased by two states when ACI was enabled; from Xe^{3+} to Xe^{5+} for the smaller clusters and from Xe^{5+} to Xe^{7+} for the larger clusters. We did find that ACI had to be enabled for our simulations to be compatible with the 2002 DESY experiment, a clear indication that ACI plays an important role in the cluster dynamics.

Afterwards, we studied the charge state spectra shape as a function of cluster size at $8 \times 10^{12} \text{ W/cm}^2$. For the shapes to be compatible with the experimental data, a spacial averaging of the intensity in the laser profile had to be performed. By allowing data from a lower intensity, both the maximum charge state (Xe^{4+}) and the most abundant one (Xe^{1+}) matched the experimental data for Xe_{90} clusters, but only when ACI was enabled. Due to computational limits, the largest cluster size simulated was $\text{Xe}_{5,083}$ (11 icosahedral shells), much smaller than the experiment's $\text{Xe}_{90,000}$ (~ 30 icosahedral shells), preventing any direct comparison.

The DESY experiment saw up to Xe^{8+} for the largest cluster size ($\text{Xe}_{90,000}$) which we could not simulate. It is not clear to us if the cluster size increase would show the increased charge states up to Xe^{8+} ; four times the cluster size (from $\text{Xe}_{1,415}$ to $\text{Xe}_{5,083}$) just doubled the yield of Xe^{5+} . Does increasing by sixty times the cluster size able to increase not only the yield of Xe^{5+} but most importantly attain the Xe^{8+} ? This is still an open question.

Finally, we looked at the potential depth influence on charge state spectra. Recombination to the ground state

had to be enabled to prevent artificial electrons heating. A deeper potential cutoff allows stronger IBH through an augmented scattering angles, resulting in an increase of the maximum charge state seen as well as the most abundant one. This increase does saturate around 27.2 eV (1 Eh).

Other groups studied the effect on the ionization spectrum of an atomic potential and found that it maximized energy absorption through IBH compared to a pure Coulombic potential shape. Such an atomic potential could be implemented in future work to validate the idea.

-
- [1] H. Wabnitz, L. Bittner, A. R. B. de Castro, R. Dharmann, P. Grtler, T. Laarmann, W. Laasch, J. Schulz, A. Swiderski, K. von Haeften, T. Mller, B. Faatz, A. Fateev, J. Feldhaus, C. Gerth, U. Hahn, E. Saldin, E. Schneidmiller, K. Sytchev, K. Tiedtke, R. Treusch, and M. Yurkov, *Nature* **420**, 4825 (2002).
 - [2] C. Jungreuthmayer, L. Ramunno, J. Zanghellini, and T. Brabec, *Journal of Physics B: Atomic, Molecular and Optical Physics* **38**, 30293036 (2005).
 - [3] C. Siedschlag and J.-M. Rost, *Physical Review Letters* **93**, 43402 (2004).
 - [4] U. Saalmann and J.-M. Rost, *Physical Review Letters* **91** (2003), 10.1103/PhysRevLett.91.223401.
 - [5] U. Saalmann, C. Siedschlag, and J.-M. Rost, *Journal of Physics B: Atomic, Molecular and Optical Physics* **39**, R39R77 (2006).
 - [6] I. Georgescu, U. Saalmann, and J.-M. Rost, *Physical Review A* **76**, 18 (2007).
 - [7] C. Greene and R. Santra, *Physical Review Letters* **91**, 14 (2003).
 - [8] R. Santra and C. Greene, *Physical Review A* **70** (2004), 10.1103/PhysRevA.70.053401.
 - [9] F. Herman and S. Skillman, *LANL* (Prentice-Hall, 1963).
 - [10] C. Bostedt, M. Adolph, E. Eremina, M. Hoener, D. Rupp, S. Schorb, H. Thomas, A. R. B. de Castro, and T. Mller, *Journal of Physics B: Atomic, Molecular and Optical Physics* **43**, 194011 (2010).
 - [11] E. Ackad, N. Bigaouette, K. Briggs, and L. Ramunno, *Physical Review A* **83**, 063201 (2011).
 - [12] E. Ackad, N. Bigaouette, and L. Ramunno, *Journal of Physics B: Atomic, Molecular and Optical Physics* **44**, 165102 (2011), arXiv:1011.5216.
 - [13] E. Ackad, N. Bigaouette, S. Mack, K. Popov, and L. Ramunno, *New Journal of Physics* **15**, 053047 (2013).
 - [14] J. E. Barnes and P. Hut, *Nature* **324**, 446449 (1986).
 - [15] P. Gibbon and G. Sutmann, in *Quantum Simulations of Complex Many-Body Systems: From Theory to Algorithms*, NIC Series, Vol. 10 (2002) p. 467506.
 - [16] J. B. West and J. Morton, *Atomic Data and Nuclear Data Tables* **22**, 103107 (1978).
 - [17] W. Lotz, *Zeitschrift fur Physik* **206**, 205211 (1967).
 - [18] H. Tawara and T. Kato, *Atomic Data and Nuclear Data Tables* **36**, 167353 (1987).
 - [19] A. Heidenreich, I. Last, and J. Jortner, *The European Physical Journal D* **35**, 567577 (2005).
 - [20] C. Bostedt, H. Thomas, M. Hoener, E. Eremina, T. Fennel, K.-H. Meiwes-Broer, H. Wabnitz, M. Kuhlmann, E. Plonjes, K. Tiedtke, R. Treusch, J. Feldhaus, A. R. B. de Castro, and T. Moller, *Physical Review Letters* **100**, 133401 (2008).
 - [21] H. Thomas, C. Bostedt, M. Hoener, E. Eremina, H. Wabnitz, T. Laarmann, E. Plnjes, R. Treusch, A. R. B. de Castro, and T. Mller, *Journal of Physics B: Atomic, Molecular and Optical Physics* **42**, 134018 (2009).
 - [22] R. D. Cowan, *Nature*, Los Alamos Series in Basic and Applied Sciences, Vol. 140 (University of California Press, 1981) Chap. 8 and 16, p. 626627.
 - [23] M. Y. Amusia, *Atomic Photoeffect* (Springer, 1990).
 - [24] J. E. Barnes, *Journal of Computational Physics* **87** (1990), 10.1016/0021-9991(90)90232-P.
 - [25] C. Bostedt, H. Thomas, M. Hoener, T. Mller, U. Saalmann, I. Georgescu, C. Gnodtke, and J.-M. Rost, *New Journal of Physics* **12** (2010), 10.1088/1367-2630/12/8/083004.
 - [26] T. Fennel, K.-H. Meiwes-Broer, J. Tiggesbunker, P. M. Dinh, and E. Suraud, *Reviews of Modern Physics* **82**, 17931842 (2010).
 - [27] M. Hoener, C. Bostedt, H. Thomas, L. Landt, E. Eremina, H. Wabnitz, T. Laarmann, R. Treusch, A. R. B. de Castro, and T. Mller, *Journal of Physics B: Atomic, Molecular and Optical Physics* **41**, 181001 (2008).
 - [28] B. Iwan, J. Andreasson, M. Bergh, S. Schorb, H. Thomas, D. Rupp, T. Gorkhover, M. Adolph, T. Mller, C. Bostedt, J. Hajdu, and N. Tmneanu, *Physical Review A* **86** (2012), 10.1103/PhysRevA.86.033201.
 - [29] H. Iwayama, A. Sugishima, K. Nagaya, M. Yao, H. Fukuzawa, K. Motomura, X.-J. Liu, A. Yamada, C. Wang, K. Ueda, N. Saito, M. Nagasono, K. Tono, M. Yabashi, T. Ishikawa, H. Ohashi, H. Kimura, and T. Togashi, *Journal of Physics B: Atomic, Molecular and Optical Physics* **43**, 161001 (2010).
 - [30] M. Krikunova, M. Adolph, T. Gorkhover, D. Rupp, S. Schorb, C. Bostedt, S. Roling, B. Siemer, R. Mitzner, H. Zacharias, and T. Mller, *Journal of Physics B: Atomic, Molecular and Optical Physics* **45**, 105101 (2012).
 - [31] T. Laarmann, A. de Castro, P. Grtler, W. Laasch, J. Schulz, H. Wabnitz, and T. Mller, *Physical Review Letters* **92** (2004), 10.1103/PhysRevLett.92.143401.
 - [32] T. Laarmann, M. Rusek, H. Wabnitz, J. Schulz, A. de Castro, P. Grtler, W. Laasch, and T. Mller, *Physical Review Letters* **95** (2005), 10.1103/PhysRevLett.95.063402.
 - [33] R. Moshhammer, Y. Jiang, L. Foucar, A. Rudenko, T. Ergler, C. Schrtter, S. Ldemann, K. Zrost, D. Fischer, J. Titze, T. Jahnke, M. Schffler, T. Weber, R. Drner, T. Zouros, A. Dorn, T. Fenger, K. Khnel, S. Dsterer, R. Treusch, P. Radcliffe, E. Plnjes, and J. Ullrich, *Physical Review Letters* **98** (2007), 10.1103/PhysRevLett.98.203001.
 - [34] D. Rupp, M. Adolph, T. Gorkhover, S. Schorb, D. Wolter, R. Hartmann, N. Kimmel, C. Reich, T. Feigl, A. R. B. de Castro, R. Treusch, L. Strder, T. Mller, and C. Bostedt, *New Journal of Physics* **14**, 055016 (2012).
 - [35] U. Saalmann, *Journal of Physics B: Atomic, Molecular and Optical Physics* **43**, 194012 (2010).

- [36] M. Schffler, K. Kreidi, D. Akoury, T. Jahnke, A. Staudte, N. Neumann, J. Titze, L. Schmidt, A. Czasch, O. Jagutzki, R. Costa Fraga, R. Grisenti, M. Smolarski, P. Ranitovic, C. Cocke, T. Osipov, H. Adaniya, S. Lee, J. Thompson, M. Prior, A. Belkacem, T. Weber, A. Landers, H. Schmidt-Bcking, and R. Drner, [Physical Review A **78**, 013414 \(2008\)](#).
- [37] Z. B. Walters, R. Santra, and C. H. Greene, [Physical Review A **74**, 43204 \(2006\)](#), [arXiv:0510187v3 \[arXiv:physics\]](#).
- [38] B. Ziaja, H. Wabnitz, F. Wang, E. Weckert, and T. Mller, [Physical Review Letters **102** \(2009\)](#), [10.1103/PhysRevLett.102.205002](#).
- [39] B. Ziaja, H. Wabnitz, E. Weckert, and T. Mller, [New Journal of Physics **10**, 043003 \(2008\)](#).
- [40] J. Zweiback, T. Ditmire, and M. Perry, [Physical Review A **59**, R3166R3169 \(1999\)](#).
- [41] M. Arbeiter and T. Fennel, [New Journal of Physics **13**, 053022 \(2011\)](#).
- [42] D. Bauer, [Journal of Physics B: Atomic, Molecular and Optical Physics **37**, 30853101 \(2004\)](#).
- [43] C. Deiss, N. Rohringer, J. Burgdrfer, E. Lamour, C. Prigent, J.-P. Rozet, and D. Vernhet, [Physical Review Letters **96** \(2006\)](#), [10.1103/PhysRevLett.96.013203](#).
- [44] F. Dorchies, T. Caillaud, F. Blasco, C. Bont, H. Jouin, S. Micheau, B. Pons, and J. Stevefelt, [Physical Review E **71** \(2005\)](#), [10.1103/PhysRevE.71.066410](#).
- [45] R. von Pietrowski, K. von Haeften, T. Laarmann, T. Mller, L. Museur, and A. V. Kanaev, [The European Physical Journal D **38**, 323336 \(2006\)](#).
- [46] A. Kramida, Y. Ralchenko, J. Reader, and N. A. Team, [“NIST Atomic Spectra Database \(ver. 5.0\),” \(2012\)](#).